ENGINEERING

Smart, soft contact lens for wireless immunosensing of cortisol

Minjae Ku[1,2]*, Joohee Kim[1,2]*, Jong-Eun Won[2]*, Wonkyu Kang[3], Young-Geun Park[1,2,4], Jihun Park[1,2,4], Jae-Hyun Lee[2,5], Jinwoo Cheon[2,5,6]†, Hyun Ho Lee[3]†, Jang-Ung Park[1,2,5]†

Despite various approaches to immunoassay and chromatography for monitoring cortisol concentrations, conventional methods require bulky external equipment, which limits their use as mobile health care systems. Here, we describe a human pilot trial of a soft, smart contact lens for real-time detection of the cortisol concentration in tears using a smartphone. A cortisol sensor formed using a graphene field-effect transistor can measure cortisol concentration with a detection limit of 10 pg/ml, which is low enough to detect the cortisol concentration in human tears. In addition, this soft contact lens only requires the integration of this cortisol sensor with transparent antennas and wireless communication circuits to make a smartphone the only device needed to operate the lens remotely without obstructing the wearer's view. Furthermore, in vivo tests using live rabbits and the human pilot experiment confirmed the good biocompatibility and reliability of this lens as a noninvasive, mobile health care solution.

INTRODUCTION

The steroid hormone, cortisol, which is known as a stress hormone, is secreted by the adrenal gland when people are stressed psychologically or physically (*1*). This secretion occurs when the adrenal gland is stimulated by adrenocorticotropic hormone, which is secreted by the pituitary gland when it is stimulated by the corticotropin-releasing hormone secreted by the hypothalamus. This serial cortisol secretion system is referred to as a hypothalamus–pituitary gland–adrenal gland axis, which is affected by chronic stress, resulting in abnormal secretion of cortisol (*2*, *3*). The accumulation of cortisol caused by the abnormal secretion of cortisol increases the concentrations of fat and amino acid, which can result in diverse severe diseases (e.g., Cushing's disease, autoimmune disease, cardiovascular complications, and type 2 diabetes) and neurological disorders (such as depression and anxiety disorders) (*2*–*7*). In contrast, abnormally low cortisol levels can lead to Addison's disease, which results in hypercholesterolemia, weight loss, and chronic fatigue (*8*). In addition, it was recently reported that plasma cortisol can be correlated to the prognosis of traumatic brain injury (*9*). Furthermore, the extent of cortisol secretion varies from person to person, and it changes continuously (*10*, *11*). Thus, developing health care systems for real-time monitoring of the cortisol level has been explored extensively over the past decade as the key to the quantitative analysis of stress levels. Although various efforts have led to the development of cortisol sensors that can measure the concentration of cortisol in blood, saliva, sweat, hair, urine, and interstitial fluid (*12*–*17*), the accurate measurement of cortisol concentrations has been limited because of the difficulties associated with the transportation and storage of cortisol as well as the instability of the biologically active cortisol in these body fluids at room temperature. In addition, these conventional sensing methods require bulky equipment for the extraction and analysis of these body fluids, which is not suitable for mobile health care systems (*12*, *18*). Therefore, the development of noninvasive and wearable sensors that can monitor cortisol concentration accurately is highly desirable for a smart health care solution. For example, the immunoassay method, which uses an antigen-antibody binding reaction, has been used extensively for electrochemical cortisol immunosensors using saliva and interstitial fluid, except tears (*12*, *14*, *19*). However, these immunosensors still require the use of bulky impedance analyzers for the analysis of the Nyquist plot from electrochemical impedance spectroscopy. Although the cyclic voltammetry (CV) technique can be used as an alternative approach for sensing cortisol, additional bulky electrochemical instruments still are necessary for analyzing the CV curves (*13*, *14*, *19*). Recently, wearable forms of cortisol sensors that use sweat were developed (*15*), but they still required bulky measurement equipment (*15*, *16*). Therefore, portable and smart sensors that can monitor the accurate concentration of cortisol in real time are highly desirable for use in mobile health care.

Among the various body fluids, tears, in particular, contain important biomarkers, including cortisol (*20*, *21*). Thus, the integration of biosensors with contact lenses is a potentially attractive candidate for the noninvasive and real-time monitoring of these biomarkers from tears (*22*–*25*). However, an approach for fabricating a smart contact lens for sensing the cortisol in tears has not been demonstrated previously. Thus, here, we present an extraordinary approach for the formation of a smart, soft contact lens that enables remote, real-time monitoring of the cortisol level in the wearer's tears using mobile phones. This smart, soft contact lens is composed of a cortisol sensor, a wireless antenna, capacitors, resistors, and integrated circuit chips that use stretchable interconnects without obstructing the wearer's view. The components of this device (except the antenna) were protected from mechanical deformations by locating each of the components on discrete, rigid islands and by embedding these islands inside an elastic layer. A graphene field-effect

[1]Nano Science Technology Institute, Department of Materials Science and Engineering, Yonsei University, Seoul 03722, Republic of Korea. [2]Center for Nanomedicine, Institute for Basic Science (IBS), Seoul 03722, Republic of Korea. [3]Department of Chemical Engineering, Myongji University, Yongin 17058, Republic of Korea. [4]School of Materials Science and Engineering, Ulsan National Institute of Science and Technology (UNIST), Ulsan 44919, Republic of Korea. [5]Advanced Science Institute, Yonsei University, Seoul 03722, Republic of Korea. [6]Department of Chemistry, Yonsei University, Seoul 03722, Republic of Korea.
*These authors contributed equally to this work.
†Corresponding author. Email: jang-ung@yonsei.ac.kr (J.-U.P.); hyunho@mju.ac.kr (H.H.L.); jcheon@yonsei.ac.kr (J.C.)

transistor (FET; with the binding of monoclonal antibody) was used as this cortisol immunosensor, which exhibited a sufficiently low detection limit, i.e., 10 pg/ml, for its sensing of cortisol in human tears in which the cortisol concentration ranges from 1 to 40 ng/ml (*26*). This sensor was integrated with a near-field communication (NFC) chip and antenna inside the soft contact lens for the real-time wireless transmission of the data to the user's mobile device (e.g., a smart phone or a smart watch). The antenna occupies a relatively large area of this soft lens, so it requires its high stretchability, good transparency, and low resistance for operating a standard NFC chip at 13.56 MHz. In our approach, the hybrid random networks of ultralong silver nanofibers (AgNFs) and fine silver nanowires (AgNWs) enabled high transparency and good stretchability of this antenna and its low sheet resistance for reliable standard NFCs (at 13.56 MHz) inside this smart contact lens. Thus, the fully integrated system of this smart contact lens provided wireless and battery-free operation for the simultaneous detection and transmission of the cortisol concentration from tears to a mobile phone using standard NFC. In addition, a human pilot trial and in vivo tests conducted using live rabbits demonstrated the biocompatibility of this lens, and its safety against inflammation and thermal/electromagnetic field radiation suggests its substantial usability as a noninvasive, mobile health care solution.

RESULTS

Cortisol immunosensor

A graphene FET sensor was fabricated by binding the cortisol monoclonal antibody (C-Mab) to the surface of graphene for the immunosensing of cortisol. Here, graphene acts as a transducer that converts the interaction between cortisol and C-Mab into electrical signals. Figure 1A shows the immobilization process of C-Mab to graphene. Immobilization proceeds through amide bonding of the C-Mab onto the carboxyl group of the graphene surface via the EDC [1-ethyl-3-(3-dimethylaminopropyl) carbodiimide hydrochloride]/NHS (*N*-hydroxysulfosuccinimide) coupling reaction. A chemical vapor deposition–synthesized graphene layer was transferred onto a desired substrate and exposed to ultraviolet ozone (UVO) to activate the surface of the graphene with the carboxylate group. Figure S1 shows the contact angle between this surface of the graphene and a droplet of deionized (DI) water. Longer exposure time to UVO can decrease the hydrophobicity of graphene with decreasing the contact angle. Table S1 shows the increase in the electrical resistance of graphene that resulted from this UVO treatment. In our experiment, 2 min of exposure time to UVO decreased the contact angle from 70° to 38° without increasing the resistance of the graphene notably. UVO exposure times longer than this threshold time degraded the resistance of the graphene excessively, so the time of exposure of our samples to UVO was limited to 2 min. Figure S2A illustrates the process of immobilizing C-Mab through the EDC/NHS coupling reaction. This two-step coupling reaction of EDC and NHS can mediate the amide bonding between the carboxylate group of the UVO-exposed graphene and the amine group of the protein (*12*, *17*, *27*, *28*). Here, EDC forms reactive *O*-acylisourea ester, thereby making the surface unstable. This *O*-acylisourea ester reacts with the NHS to form amine-reactive NHS ester with the surface still remaining semistable. Then, C-Mab with the amine group reacts with the amine-reactive NHS ester, thereby forming stable amide bonding that can immobilize C-Mab to the NHS on the surface of the graphene. Figure S2B shows the Fourier transform infrared (FTIR) spectroscopy spectra of the DI water after the cortisol sensor had been immersed for 24 hours. The spectra of the DI water in which the sensor was immersed were not significantly different from those of the pristine DI water. However, the C-Mab solution that had a concentration of 1 μg/ml had a significant peak intensity in the range of 3000 to 2800 cm^{-1}, representing the N-H bonding in the C-Mab. These results indicated that C-Mab formed stable bonding on the carboxylated graphene and was negligibly detached by exposure to water.

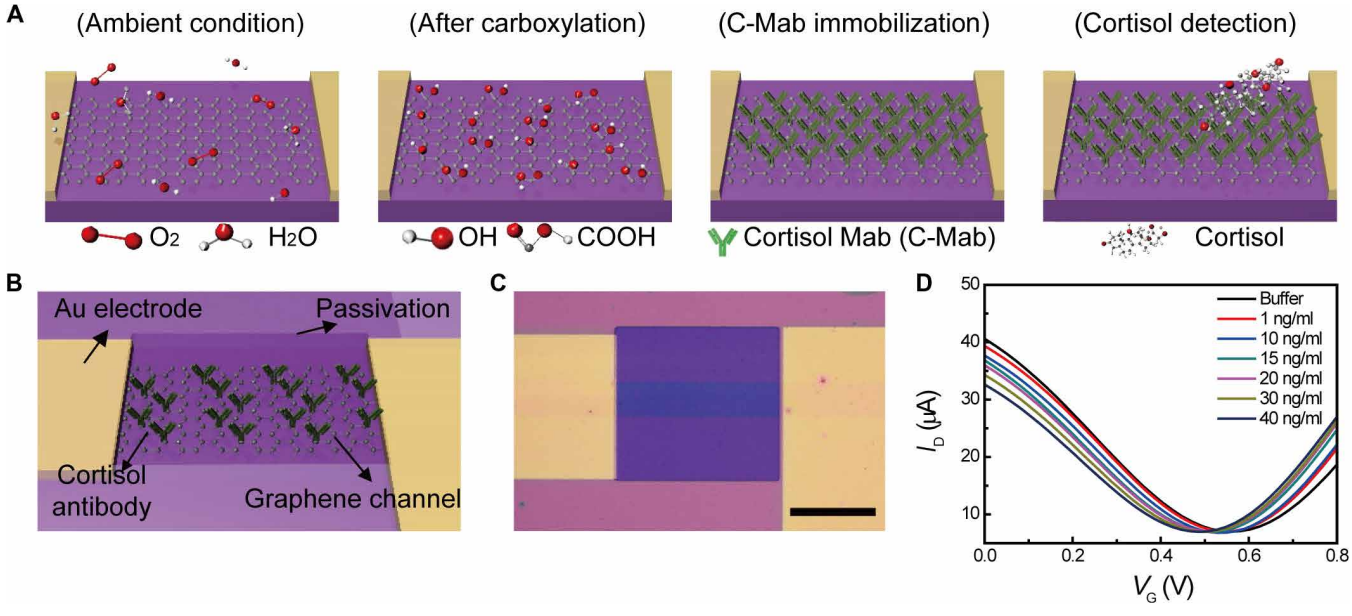

Fig. 1. Cortisol immunosensor. (**A**) Process of C-Mab immobilization. (**B**) Schematic image of the graphene FET structure. (**C**) Optical microscope image of the fabricated graphene FET device. Scale bar, 200 μm. (**D**) Transfer curve of the drain current according to the gate voltage.

The graphene FET where the graphene channel is selectively functionalized with C-Mab can be used as a cortisol sensor. Figure 1 (B and C) shows the schematic and the optical micrographs of this cortisol sensor, respectively. With the exception of the square-shaped areas that were used to expose the graphene channel, the source/drain electrodes and interconnects were passivated with a 500-nm-thick epoxy layer (SU-8, MicroChem Inc.). Supplementary Materials and Methods provide the detailed steps that were used to fabricate this graphene FET sensor. After preparing a solution of artificial tears that also included specific concentrations of cortisol, the solution was dropped on the graphene channel to measure the drain current by applying the gate voltage using an Ag/AgCl probe for the characterization of this cortisol sensor. Figure 1D shows the transfer curve of this graphene FET with the bipolar characteristic for various concentrations of the cortisol. Cortisol has the isoelectric point from pH 5.2 to pH 5.4; therefore, it is negatively charged under physiological condition (between pH 7.35 and pH 7.45) (*29*). Thus, electrons can be injected from adsorbates into the graphene channel (*30*–*32*). Therefore, the graphene channel (p-type) decreases its major carrier concentration, and thus, the drain current decreases at a higher concentration of cortisol. Furthermore, for further information about the reproducibility of the sensors, the data obtained from the 10 samples are provided in fig. S3. As shown in fig. S3, our sensors presented reproducible characteristics in conductance versus gate potential at varied concentration.

In vitro tests

On the basis of the transfer characteristic, the drain currents for cortisol concentrations ranging from 1 to 40 ng/ml were measured in real time at zero gate bias (V_G = 0 V) and at a drain bias (V_D) of 0.1 V (Fig. 2A). For this measurement, a polydimethylsiloxane microfluidic channel was located on the cortisol sensor to flow the cortisol solutions with various concentrations at the constant flow rate of 1 ml/hour as shown in fig. S4A. (The steps used to fabricate this microfluidic channel are also described in Supplementary Materials and Methods.) Although the drain current was preserved consistently without changing the concentration of cortisol, increases in the cortisol concentration instantly decreased the drain current. The limit of detection (LOD) at the signal-to-noise ratio of 3 was 10 pg/ml. Compared to the cortisol concentration of human tears in the range of 1 to 40 ng/ml, this cortisol sensor exhibited a sufficiently low LOD of 10 pg/ml. As shown in the calibration curve in Fig. 2B, the sensor was highly responsive to the typical range of cortisol concentrations in the tears (1 to 40 ng/ml), and the current decreased linearly with the concentration of the cortisol. Figure S4B shows the calibration curve of the cortisol concentration sensed from the drain current of this sensor (V_D = 0.1 V). The sensitivity of this sensor was calculated as 1.84 ng/ml per 1% of the change in its resistance. Figure 2C shows that repeating the measurements in the artificial tear fluids or in the buffer fluids did not degrade the sensitivity. The results confirmed that our cortisol sensor can operate effectively, even in the presence of ions and other interfering molecules in tears such as ascorbic acid, lactate, and urea (fig. S4C). We also investigated the thermal stability of the sensors. The cortisol sensors were stored at room temperature (22°C) or body temperature (36.5°C) for up to 192 hours, and their responses to cortisol at various concentrations were tested (Fig. 2D). No degradation of the sensitivity occurred when the sensors were stored at room temperature or at body temperature for up to 192 hours, which indicated that the enzymes remained active for at least 192 hours.

Soft contact lens for mobile wireless communications

The smart contact lens should have the capability of monitoring the cortisol concentration in tears and the capability of transmitting this information wirelessly to users' mobile devices, such as smartphones and smart watches. Among the standard wireless communication technologies, NFC can be suitable for the smart contact lens because it allows a wireless supply of power to a sensor for its battery-free operation, and it allows the wireless transmission of data with sufficient bandwidth (*33*, *34*). In contrast with the previous results of smart contact lenses for which the NFC technique was not used (*28*, *35*–*37*), our contact lens system uses this NFC function with the stretchable integration of an NFC chip (NHS 3152, NXP Semiconductors, Netherlands), a transparent antenna, capacitor, and resistor and the cortisol sensor. Figure 3A illustrates this wireless circuit diagram based on the passive communication mode of NFC for the battery-less operation of our smart lens. In this mode, the user's external mobile device, which is acting as the initiator, applies a magnetic field to the target antenna inside our contact lens. This antenna is an *LC* circuit that consists of an inductor and a capacitor, and the inductor acts as a coil to induce current by the magnetic field. Then, the NFC chip can operate to read the resistance of the cortisol sensor and to transmit these data wirelessly to smartphones, smart watches, or tablet computers. Bias voltage is applied by a digital-to-analog converter (DAC), and the voltage is read by an analog-to-digital converter (ADC). A resistor is integrated in the circuit to read the change in the resistance of the cortisol sensor based on the reference resistance. A more detailed method for calculating the cortisol concentration is explained in Materials and Methods.

The wireless operations of the commercial NFC platform are standardized for the frequency of 13.56 MHz to avoid high crosstalk and attenuation. Thus, the antenna that will occupy a large portion of the soft contact lens must have low sheet resistance (R_s) for the wireless operation of the standardized NFC chip at 13.56 MHz, and it also must have good transparency and stretchability. However, the small size of a contact lens and the relatively high R_s of conventional transparent electrodes limit the antenna design for standardized NFC conditions. Figure 3 (B and C) shows that our stretchable and transparent antenna was fabricated using random networks of AgNFs and AgNWs. This antenna was designed to fit the size of a commercial contact lens for the NFC operation at 13.56 MHz (inner diameter of the coil, 2.325 mm; outer diameter, 5.75 mm; number of turns, 9; width, 300 μm; interval between turns, 50 μm). For the formation of the AgNF-AgNW hybrid network, continuous networks of AgNFs were electrospun using a suspension of Ag nanoparticle ink (Nano-CoIn, NPK Co. Ltd.) in ethylene glycol (*38*). After thermal annealing at 150°C for 30 min, conductive AgNFs were formed with an average diameter of 467 ± 47 nm. These ultralong AgNFs were advantageous for reducing the R_s of their networks while maintaining large vacant areas in networks for high transparency (*38*). However, these large open spaces can increase the resistance of the AgNF networks substantially when they are patterned as fine geometries of the antennas with narrow widths. This occurred because locally disconnected areas were produced at the edges of the pattern by the photolithographic etching of the AgNFs. Therefore, finer AgNWs (average diameter, 30 ± 5 nm; average length, 25 ± 5 μm) were coated on top of these AgNF networks to bridge across the locally disconnected, open areas of the AgNF networks to preserve the resistance of these narrow antenna patterns.

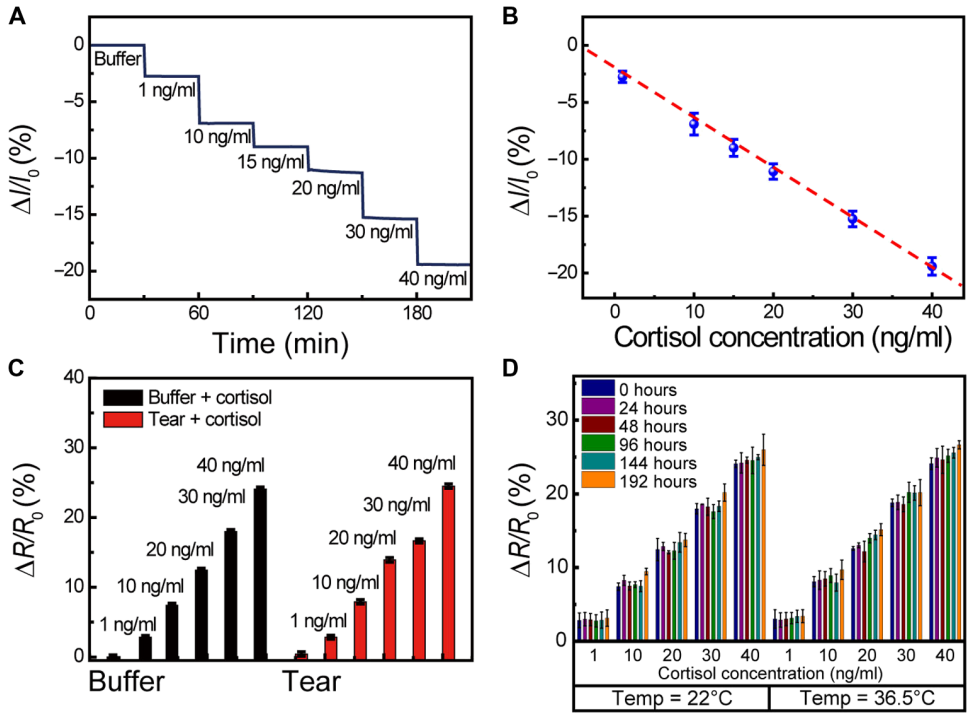

Fig. 2. In vitro tests. (**A**) Real-time, relative current change at gate voltage $V_G = 0$ V and drain voltage $V_D = 0.1$ V. (**B**) Calibration curve of the relative current change according to the cortisol concentration. (**C**) Relative resistance change according to the cortisol concentration in the buffer and the artificial tear solvent. (**D**) Relative change in the resistance of the sensor according to the cortisol concentration at 22°C and at 36.5°C. Each data point indicates the average for 10 samples, and the error bars represent the SDs.

The detailed method for the formation of AgNF-AgNW hybrid networks is described in Supplementary Materials and Methods. As a transparent antenna for the standardized NFC operations at 13.56 MHz, the AgNF-AgNW networks were formed by the electrospinning of AgNFs for 10 s with successive spraying of AgNWs for 60 s, which resulted in their having an average R_s of 0.3 ± 0.08 ohm per square and a transparency of 71% at 550 nm (Fig. 3D). Figure S5A also verifies that this transparency was sufficient to read letters (on a paper) under the antenna. Figure 3E presents the good mechanical stretchability of this AgNF-AgNW antenna. The relative change in its resistance was negligible under a tensile strain of 30%, and this stretchability is suitable for a soft contact lens that has to be turned inside out. In addition, the stretching test with 300 stretching-relaxing cycles (to 30% in tensile strain) did not degrade its resistance notably. Figure 3F shows that the resonance frequency of this antenna sample became centered close to 13.56 MHz after its connection to a 180-pF capacitor for the standardized NFC condition. A quality (Q) factor means the ratio of the frequency selectivity to a given frequency (*39*). The resulting antenna exhibited a high Q factor value of ~3.9 for the transmission distance (to a smartphone) of ~7 mm. The passivation of this AgNF-AgNW antenna by coating a parylene elastomeric cover layer (thickness, 1 μm) could retard the Ag oxidation. Although this passivated antenna sample was immersed in a phosphate-buffered saline (PBS) or artificial tear solution, its resonance properties were not degraded notably. In addition, the accelerated aging test was performed at the aging temperature of 70°C to investigate the long-term stability of this smart contact lens. For this test, the antenna was stored in air for up to 16 days, which corresponded to the storage period of 1 year. Then, the antenna was characterized using a network analyzer. As shown in fig. S5, B and C, the contact lens device operated reliably and showed negligible degradation during the accelerated aging.

Stretchable integrations for a soft contact lens

For the formation of a soft, smart contact lens, all components of the cortisol sensor, antenna, NFC chip, capacitor, and resistor must be integrated electrically with stretchable interconnections. The softness of contact lenses can lead to fractures in the conventional brittle and rigid materials for the integrated electronic system, which could damage the cornea or the eyelid. In our approach, we formed a soft contact lens with highly transparent and stress-tunable hybrid geometries composed of rigid islands for locating the components of the device (such as the cortisol sensor, NFC chip, capacitor, and resistor) and elastic joints for locating a stretchable, transparent antenna and interconnection electrodes. The rigid segments were patterned using a thin, photopatternable optical polymer (SPC-414, EFiRON), and the elastic parts were made of a silicone elastomer (Elastofilcon A, CooperVision), which is a conventional material for soft contact lenses. The detailed fabrication process of the rigid-soft hybrid substrates is provided in Materials and Methods. After forming a flat film of this rigid-soft hybrid material with locating devices, all of the components of the cortisol sensor device, i.e., the NFC chip, capacitor, resistor, and antenna, were connected electrically by printing a liquid metal of an eutectic gallium-indium alloy [75 weight % (wt %) Ga and 25 wt % In; Changsha Santech Materials Co. Ltd.] with a narrow linewidth (<10 μm). High-resolution, direct printing of a liquid metal through a nozzle at ambient conditions was used to form stretchable patterns of these interconnects (*40*, *41*). After the full integration, the molding of the resulting flat sample (with devices) into the curved shape of a lens by injecting a precursor of

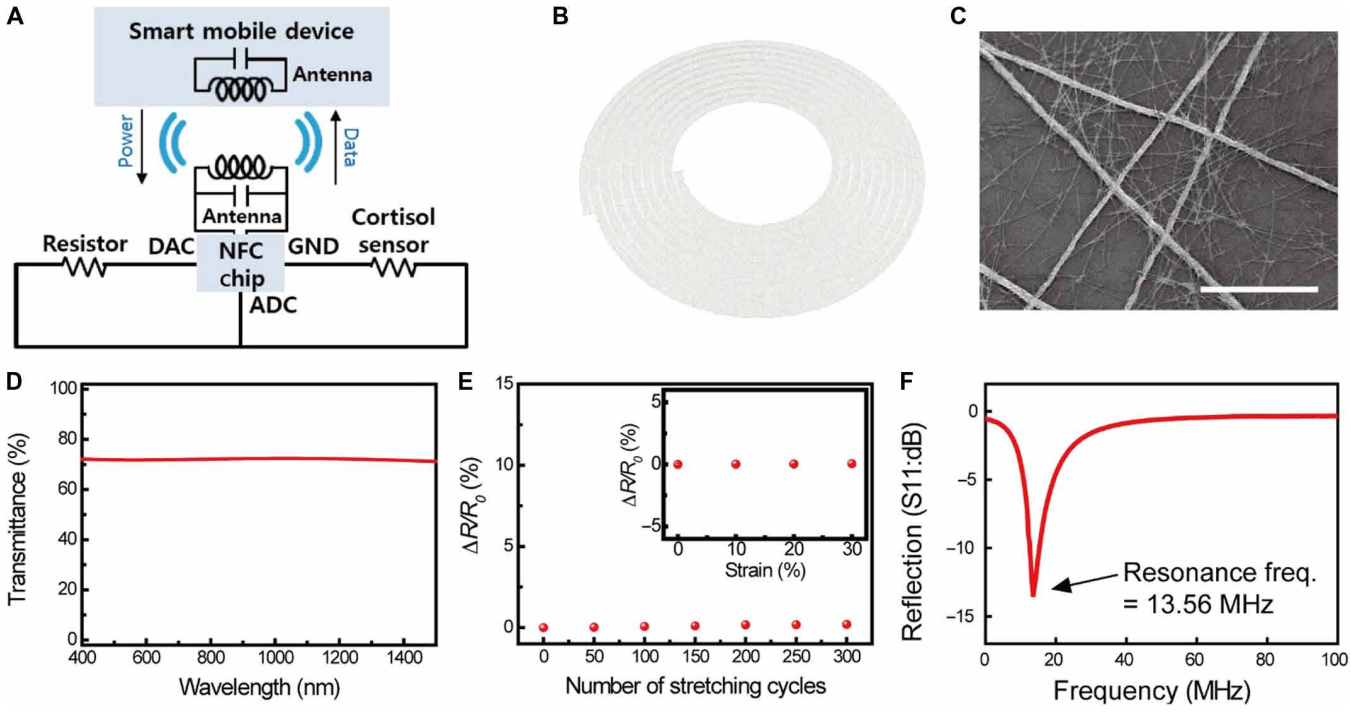

Fig. 3. NFC and stretchable and transparent AgNF-AgNW hybrid antenna. (**A**) Circuit diagram connected with NFC chip, cortisol sensor, and components including antenna and resistor. (**B**) Schematic illustration of the stretchable and transparent antenna for wireless communications. (**C**) Scanning electron microscopy image of random networks of AgNF-AgNW hybrid structure. Scale bar, 20 μm. (**D**) Transparency of the AgNF-AgNW hybrid patterned antenna coil. (**E**) Stretching-relaxing cycle test conducted up to 300 times of the AgNF-AgNW hybrid with negligible strain up to 30% (inset: AgNF-AgNW hybrid electrode strain test). (**F**) The resonance frequency of the patterned antenna resulting in 13.56 MHz.

silicone elastomer completed the fabrication of the soft, smart contact lens. During this molding step, the graphene channel was open and locally uncovered by the lens material (silicone elastomer) to allow physical contact of the channel with tears. In this way, all of the devices could be embedded inside the soft contact lens with this opening remaining for the sensor. More details of this fabrication procedure are provided in Supplementary Materials and Methods and in fig. S6. Figure 4A shows a schematic illustration of the resulting smart contact lens for monitoring cortisol in tears, and Fig. 4B shows photographs of the lens. This contact lens, which was based on the rigid-soft hybrid geometry in which the rigid polymeric islands were embedded inside an elastic layer, can effectively distribute the mechanical strain and protect the electronic components from mechanical deformations of the soft lens. The elastic moduli (E) between the rigid and the soft parts are large enough to concentrate the stretching stress on the soft area of this lens, i.e., the E of Elastofilcon A is ~0.09 MPa and the E of the optical polymer is ~360 MPa (*42*). As a result, the sensor was placed on the rigid island embedded inside the layer of soft contact lens (fig. S7A). This layout allowed the sensor to be isolated mechanically from the strain of the soft contact lens, and it had only a negligible change in resistance (fig. S7B). In addition, for the transparency of the lens, the optical indices of refraction (n) of the two heterogeneous materials are similar (n of Elastofilcon A, 1.41; n of the optical polymer, 1.407). Figure 4C shows the transparency and haziness curves of a flat film of this rigid-soft hybrid (thickness of Elastofilcon A, 100 μm; thickness of optical polymer, 50 μm). This hybrid substrate exhibited good transmittance (~93% at 550 nm) with low haze (~1.2% at 550 nm). As an example, fig. S7C presents a photo of this contact lens (where no components of the device were included), and the boundaries of these two different materials (optical polymer and Elastofilcon A) could hardly be seen. In addition, no gaps at the interfaces between these heterogeneous regions were generated, even during the stretching states (30% in tensile strain). Figure S7D shows that the optical transparency and haze of the integrated contact lens were also measured as 67 and 10.0%, respectively (at 550 nm). In addition, since all of the components of the device are placed outside the wearer's pupil, there is minimal interference with the wearer's field of vision. Therefore, our contact lens can reduce the adverse effect on the wearer's vision. Figure 4D shows that the resonance characteristic of the antenna (embedded inside this lens) was maintained reliably before and after reversing the soft lens. In addition, a parylene elastomeric passivation layer (thickness, 1 μm) encapsulated the AgNF-AgNW antenna of this contact lens to avoid the oxidation of Ag. Although this smart contact lens was immersed inside a PBS solution (pH 7.4) or an artificial tear solution for 192 hours, the resonance properties of the antenna were not degraded notably (Fig. 4E).

In vivo tests

Figure 5A and movie S1, respectively, show a photograph and a movie of a 24-year-old female subject wearing the fully integrated, smart contact lens that allowed real-time, wireless sensing of cortisol using a mobile phone. Figure S8A shows the variation of the concentrations of cortisol for a human subject as a function of time. The cortisol concentration changed slightly during the measurement period, which was similar to the range of variation reported in a previous paper (*26*). Figure 5B shows a schematic illustration of

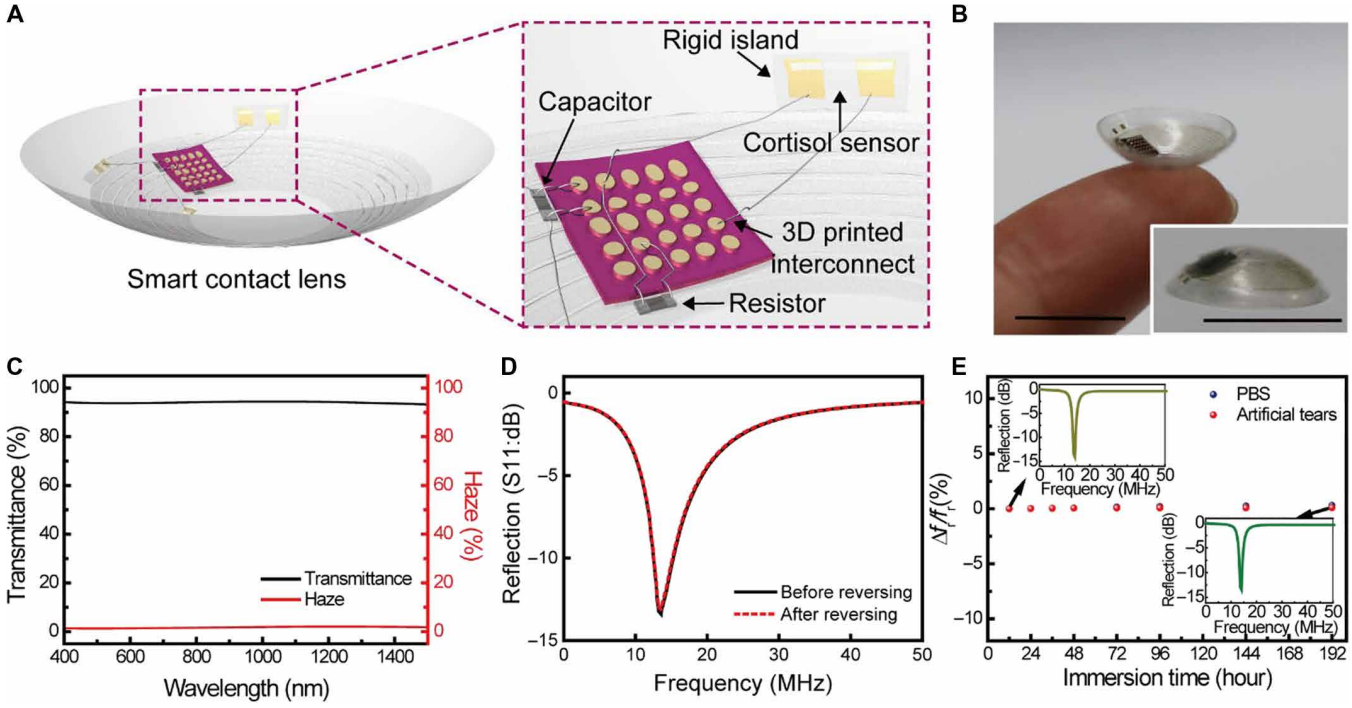

Fig. 4. Smart contact lens packaging. (**A**) Schematic of the packaged smart contact lens integrated with three-dimensional (3D) printed stretchable interconnects and cortisol sensor located on the rigid island. A capacitor and a resistor were integrated for resonance frequency and reference resistance, respectively. (**B**) Photograph of the smart contact lens that was fabricated (inset: close-up outer image of the smart contact lens). Scale bars, 1 cm. (**C**) Optical transmittance and haziness of the rigid-soft hybrid material. (**D**) Radiation characteristics before and after reversion of the stretchable antenna. (**E**) Relative resonance frequency change immersed in the PBS and artificial tears up to 192 hours (inset: radiation characteristics of the antenna after immersion tests in artificial tears for 12 and 192 hours, respectively). Photo credit: (B) Minjae Ku, Yonsei University.

this lens by wirelessly transmitting data to a reader (such as a smartphone) through the standard NFC interface. The wireless delivery of power from the smartphone can provide the ac bias to operate the logic chip for evaluating the sensor's response, and this logic chip includes an ADC and all computing functionality for both recording high-speed data and the real-time, wireless transmission of the sensor's output. In the design of this contact lens, the placement of all of the components of the device did not screen the wearer's pupil, so it minimized the interference with the wearer's field of vision. Figure 5 (C and D) shows the results of the simulation for a specific absorption rate (SAR) for a person, which indicated that the maximum SAR value of this contact lens was only 0.102 W/kg. This value was comparable to the level of the electromagnetic waves from a smartphone (0.14 to 0.33 W/kg), and it was about 20 times lower than the regulation value (2 W/kg) (*43*). In addition, a slit-lamp examination was performed for the person's eye after wearing this lens for 12 hours. Figure 5E shows the slit-lamp images with fluorescein staining, which indicates that there was no overt reaction of the person's cornea to this smart lens. In addition, the conjunctival area of the person's eye was examined before and after wearing the lens for 12 hours. As fig. S8B shows, no substantial conjunctival injection was observed after this length of time. As another in vivo test, an artificial tear solution with the cortisol concentration of 20 ng/ml was dropped onto the contact lens after it was placed on a live rabbit's eye (movie S2). For this experiment, a manufactured cortisol solution (C106; Sigma-Aldrich) and a commercial artificial tear solution were mixed with this desired concentration for 1 min at room temperature before administering this eye drop. This was done because the cortisol concentration in the plasma of rabbits is much lower than that of people, and the cortisol sensor was calibrated to measure the cortisol concentration in people (*44*). After wearing this contact lens during the threshold period for antigen-antibody reaction, the cortisol concentration was detected wirelessly through the automatic calibration in the software of a smartphone and then quantitatively displayed on the screen of the mobile phone. Figure 5F shows that the cortisol concentrations measured using the contact lens sensor had a good correlation with the concentrations of the manufactured cortisol solutions. The rabbit did not show abnormal behavior while wearing the lens, and this contact lens remained stable against the repetition of its eyeblinks. We also used an IR camera to monitor the heat that was generated while the rabbit was wearing the lens (fig. S9A and movie S3). In this case, instead of a mobile phone, an external metallic coil was used for the wireless transmission of power to the antenna of this contact lens through the air gap of ~5 mm, as illustrated in fig. S9 (B and C). While the power was being transmitted for the operation of this lens circuit, the fluctuation of heat was negligible (ΔT ~ 0.5°C) because of its magnetic coupling at the low-frequency band (13.56 MHz). Although the temperature of the transmitting coil increased by ~0.5°C for its power transfer to the lens, its wireless function prevented this coil from touching the rabbit's eye or eyelid with the air gap of ~5 mm. The cytotoxicity of this contact lens was also tested by measuring the viability of human dermal fibroblast cells. The cytotoxicity test was conducted using the WST-8 assay for quantifying the surviving cells by detecting

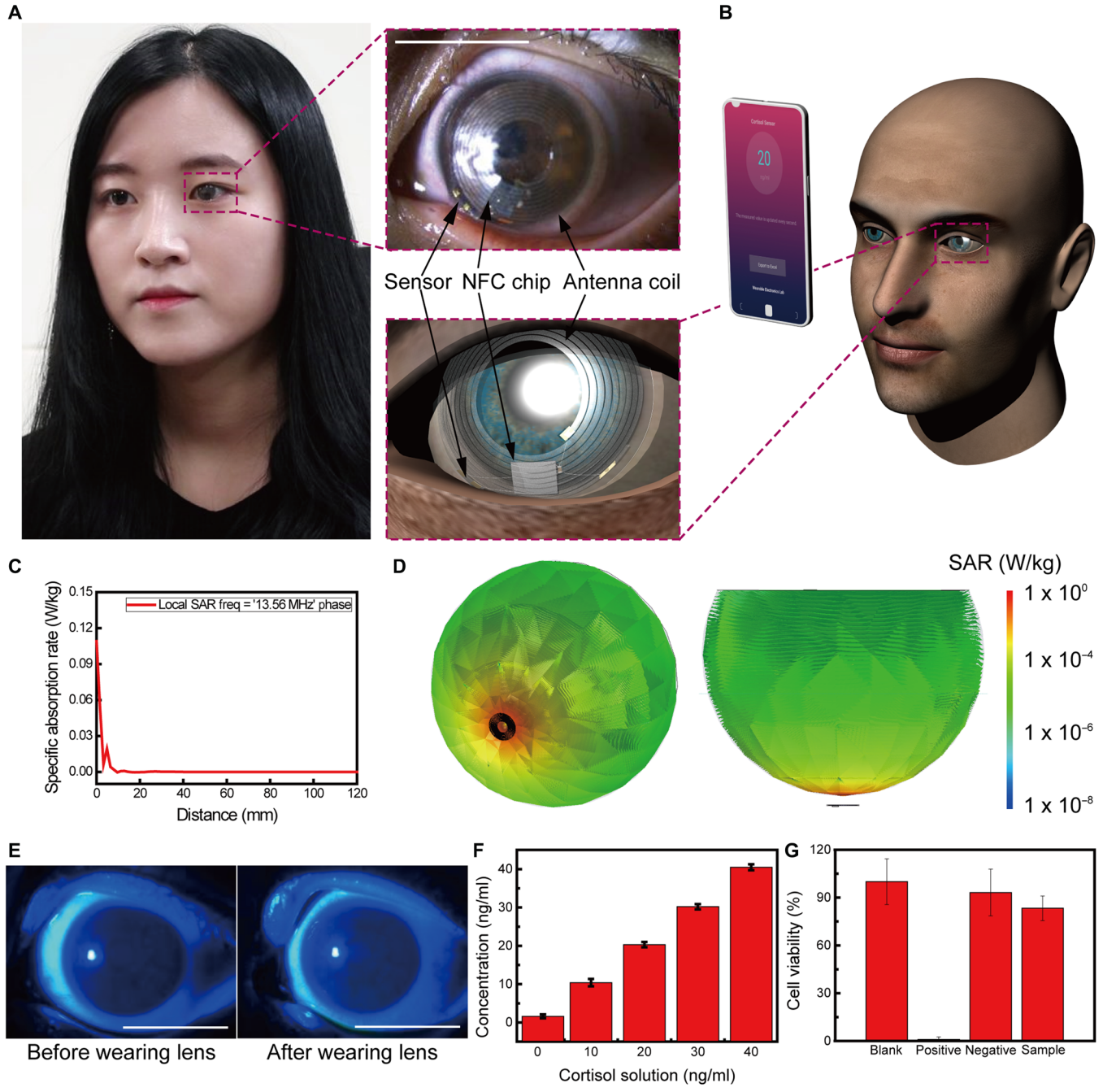

Fig. 5. In vivo tests. (**A**) Photograph of an adult woman wearing the smart contact lens on her left eye (inset: close-up image of the smart contact lens on the eye). (**B**) Schematic image of the cortisol level measurement using the smart contact lens. (**C** and **D**) SAR that resulted from the simulation. (**E**) Slit-lamp images of a human eye with fluorescein staining before and after wearing the smart contact lens. Scale bars, 1 cm. (**F**) Cortisol concentration measured using the contact lens sensor as a function of the concentration of the cortisol solution that was dropped into the eye. Each data point indicates the average for 10 samples, and the error bars represent the SDs. (**G**) Cytotoxicity test of the smart contact lenses. Photo credits: (A) Joohee Kim, Yonsei University and (E) Minjae Ku, Yonsei University.

biological responses after incubating the cells in the extracts of the test samples and controls. The extracts were prepared by incubating the sample in the minimum essential medium (1× MEM; Gibco) with 10% serum (horse serum; Gibco) at the conditions of 37 ± 1°C and 5 ± 1% CO_2 for 48 hours. The extract rate was set to 0.2 g/ml, which corresponded to the irregular model of solid medical devices. The experimental method is explained in more detail in Materials and Methods. Figure 5G shows the cell viability of the test sample, the blank, and the negative and positive controls. The cell viability of the test sample (with our contact lens) was 83.3%, which was comparable to the cases of commercially available soft contact lenses that included no electronic devices (cytotoxicity standardization by

ISO 109943-5:2009). Therefore, it was concluded that the smart contact lens used to monitor the cortisol level was not substantially cytotoxic to people.

DISCUSSION

We demonstrated the fabrication of a soft, smart contact lens for the wireless and quantitative detection of the cortisol concentration in tears. For this immunosensing of cortisol, a FET sensor with its graphene channel chemically bonded with the C-Mab was integrated with the NFC device and the transparent, stretchable antenna inside the soft contact lens. This fully integrated system of a smart contact lens enabled its wireless and battery-free operation without any necessity for other external equipment other than a smartphone to monitor signals from this lens. In addition, the pilot trial with a person and the in vivo tests with live rabbits verified the good biocompatibility of this smart lens as a noninvasive mobile health care solution that can provide clinical information and the potential capability for machine learning in diagnosing disease. Clinical analyses on the correlation of the cortisol level in the tears with the serum case, as well as with other biomarkers at various physiological conditions, appear to be a promising direction for future work.

MATERIALS AND METHODS

Calculation of cortisol concentration

The concentration of cortisol was calculated from the change in the resistance of the sensor. Thus, the measurement process was performed after adjustment, i.e., measuring the resistance of the zero concentration. The change in the resistance was calculated using the following equation

$$\Delta R/R_0 = \left[\frac{R_{\mathrm{Ref}} V_{\mathrm{ADC2}}}{V_{\mathrm{DAC}} - V_{\mathrm{ADC2}}} - \frac{R_{\mathrm{Ref}} V_{\mathrm{ADC1}}}{V_{\mathrm{DAC}} - V_{\mathrm{ADC1}}}\right] \Big/ \frac{R_{\mathrm{Ref}} V_{\mathrm{ADC1}}}{V_{\mathrm{DAC}} - V_{\mathrm{ADC1}}} \quad (1)$$

where V_{ADC} and V_{DAC} are the measured voltage and the applied voltage, respectively, and R_{Ref} is the resistance of the resistor integrated with the NFC chip. The cortisol concentration can be calculated using following equation

$$\text{Cortisol concentration} = 1.84 \times \Delta R/R_0 - 4.23 \quad (2)$$

where the concentration has the units of ng/ml.

Rigid-soft hybrid film

A Ni/Cu (10/1 μm) sacrificial layer (thickness of 300 nm; MicroChem Corporation) was deposited on the SiO_2 wafer through electron beam evaporation. Then, parylene (1 μm) was deposited on the sacrificial layer, and the Au source/drain part of the sensor was deposited and patterned. Subsequently, an optical polymer (SPC-414, EFiRON) was spun (1500 rpm for 30 s) for its thickness of 50 μm, and it was photolithographically patterned to the rigid island structure. Then, an elastomer (Elastofilcon A, CooperVision) mixed with a base and a curing agent using the weight ratio of 10:1 was spun (1000 rpm for 30 s; the thickness of 100 μm) and thermally cured at 100°C for 1 hour (film thickness, 5 μm). As the last step, the sacrificial layer was removed by wet etching using the etchant of $FeCl_3$/HCl/ H_2O [1:1:20 (v/v)] to delaminate the film from the SiO_2 wafer.

Cell culture and cytotoxicity assay

Normal human dermal fibroblast cells (PromoCell) were maintained in Cascade Biologics Medium 106 (Gibco), supplemented with Low Serum Growth Supplement (Gibco) (complete medium) at 37°C in a humidified atmosphere of 5% CO_2 with medium change every 3 days. When the confluence was closed in 80%, the cells were subcultured with 0.025% trypsin/EDTA (Gibco) and incubated in the complete medium condition. At fourth passage, these cells were harvested and plated at a density of 5000 cells per well in each well of 96-well plates. The cells were incubated in complete medium for 24 hours.

For the cytotoxicity test, the process was performed in accordance with ISO 10993-5. We selected the human dermal fibroblast cell because of its high sensitivity to chemicals in the cytotoxicity test and because of the abundant data that are available related to the cytotoxicity test. In this experiment, our smart contact lens was compared in both polyurethane films containing 0.1% zinc diethyldithiocarbamate (Hatano Research Institute) and high-density polyurethane film (Hatano Research Institute) as a positive and negative control. Before the experiment, all contact lenses were sterilized in 70% ethanol for 30 min and the samples were then dried in a hood. Each sample ($n = 4$) was immersed and incubated in complete medium at 37°C for 48 hours. The condition for extracts was prepared with contact lens of 0.2 g in complete medium of 1 ml. The pretreated medium of incubated cells was changed to extracted medium immersed with contact lenses. The cells treated with extracted medium were incubated for 24 hours. The cytotoxicity was assessed by Cell Counting Kit-8 assay (Dojindo). The procedure in the instructions was followed. The absorbance was read at 450 nm using multimode plate reader (PerkinElmer). The absorbance values were converted into percentage values about the blank obtained from only cell growth media.

Rabbit experiments

In vivo tests were conducted on the basis of the guidelines of the National Institutes of Health for the care and use of laboratory animals and with the approval of the Institute of Animal Care and Use Committee of Ulsan National Institute of Science and Technology (UNIST) and the Institute of Animal Care and Use Committee of Yonsei University (UNISTIACUC-18-02 and IACUC-A-201910-963-01). The Institute of Animal Care and Use Committee of UNIST and the Institute of Animal Care and Use Committee of Yonsei University were the ethics review committee.

SUPPLEMENTARY MATERIALS

Supplementary material for this article is available at http://advances.sciencemag.org/cgi/content/full/6/28/eabb2891/DC1

REFERENCES AND NOTES

1. F. Holsboer, M. Ising, Stress hormone regulation: Biological role and translation into therapy. *Annu. Rev. Psychol.* **61**, 81–109 (2010).
2. E. R. de Kloet, M. Joëls, F. Holsboer, Stress and the brain: From adaptation to disease. *Nat. Rev. Neurosci.* **6**, 463–475 (2005).
3. S. H. Sunwoo, J. S. Lee, S. Bae, Y. J. Shin, C. S. Kim, S. Y. Joo, H. S. Choi, M. Suh, S. W. Kim, Y. J. Choi, T.-i. Kim, Chronic and acute stress monitoring by electrophysiological signals from adrenal gland. *Proc. Natl. Acad. Sci. U.S.A.* **116**, 1146–1151 (2019).
4. J. Newell-Price, X. Bertagna, A. B. Grossman, L. K. Nieman, Cushing's syndrome. *Lancet* **367**, 1605–1617 (2006).
5. L. Stojanovich, Stress and autoimmunity. *Autoimmun. Rev.* **9**, A271–A276 (2010).
6. B. S. McEwen, Protective and damaging effects of stress mediators. *N. Engl. J. Med.* **338**, 171–179 (1998).

7. F. A. J. L. Scheer, M. F. Hilton, C. S. Mantzoros, S. A. Shea, Adverse metabolic and cardiovascular consequences of circadian misalignment. *Proc. Natl. Acad. Sci. U.S.A.* **106**, 4453–4458 (2009).
8. O. M. Edwards, R. J. Courtenay-Evans, J. M. Galley, J. Hunter, A. D. Tait, Changes in cortisol metabolism following rifampicin therapy. *Lancet* **2**, 548–551 (1974).
9. X. Saichan, C. Wei, F. Qinglong, W. Jun, X. Lei, Plasma cortisol as a noninvasive biomarker to assess severity and prognosis of patients with craniocerebral injury. *Eur. Rev. Med. Pharmacol. Sci.* **20**, 3835–3838 (2016).
10. R. Thun, E. Eggenberger, K. Zerobin, T. Lüscher, W. Vetter, Twenty-four-hour secretory pattern of cortisol in the bull: Evidence of episodic secretion and circadian rhythm. *Endocrinology* **109**, 2208–2212 (1981).
11. R. M. Sapolsky, Individual differences in cortisol secretory patterns in the wild baboon: Role of negative feedback sensitivity. *Endocrinology* **113**, 2263–2267 (1983).
12. A. Kaushik, A. Vasudev, S. K. Arya, S. K. Pasha, S. Bhansali, Recent advances in cortisol sensing technologies for point-of-care application. *Biosens. Bioelectron.* **53**, 499–512 (2014).
13. P. K. Vabbina, A. Kaushik, N. Pokhrel, S. Bhansali, N. Pala, Electrochemical cortisol immunosensors based on sonochemically synthesized zinc oxide 1D nanorods and 2D nanoflakes. *Biosens. Bioelectron.* **63**, 124–130 (2015).
14. A. Singh, A. Kaushik, R. Kumar, M. Nair, S. Bhansali, Electrochemical sensing of cortisol: A recent update. *Appl. Biochem. Biotech.* **174**, 1115–1126 (2014).
15. O. Parlak, S. T. Keene, A. Marais, V. F. Curto, A. Salleo, Molecularly selective nanoporous membrane-based wearable organic electrochemical device for noninvasive cortisol sensing. *Sci. Adv.* **4**, eaar2904 (2018).
16. D. Kinnamon, R. Ghanta, K.-C. Lin, S. Muthukumar, S. Prasad, Portable biosensor for monitoring cortisol in low-volume perspired human sweat. *Sci. Rep.* **7**, 13312 (2017).
17. Y.-H. Kim, K. Lee, H. Jung, H. K. Kang, J. Jo, I.-K. Park, H. H. Lee, Direct immune-detection of cortisol by chemiresistor graphene oxide sensor. *Biosens. Bioelectron.* **98**, 473–477 (2017).
18. T. Stalder, S. Steudte, N. Alexander, R. Miller, W. Gao, L. Dettenborn, C. Kirschbaum, Cortisol in hair, body mass index and stress-related measures. *Biol. Psychol.* **90**, 218–223 (2012).
19. S. K. Arya, A. Dey, S. Bhansali, Polyaniline protected gold nanoparticles based mediator and label free electrochemical cortisol biosensor. *Biosens. Bioelectron.* **28**, 166–173 (2011).
20. N. M. Farandos, A. K. Yetisen, M. J. Monteiro, C. R. Lowe, S. H. Yun, Contact lens sensors in ocular diagnostics. *Adv. Healthc. Mater.* **4**, 792–810 (2015).
21. B. A. Cardinell, M. L. Spano, J. T. La Belle, Toward a label-free electrochemical impedance immunosensor design for quantifying cortisol in tears. *Crit. Rev. Biomed. Eng.* **47**, 207–215 (2019).
22. J. Park, D. B. Ahn, J. Kim, E. Cha, B.-S. Bae, S.-Y. Lee, J.-U. Park, Printing of wirelessly rechargeable solid-state supercapacitors for soft, smart contact lenses with continuous operations. *Sci. Adv.* **5**, eaay0764 (2019).
23. J. Kim, M. Kim, M.-S. Lee, K. Kim, S. Ji, Y.-T. Kim, J. Park, K. Na, K.-H. Bae, H. K. Kim, F. Bien, C. Young Lee, J.-U. Park, Wearable smart sensor systems integrated on soft contact lenses for wireless ocular diagnostics. *Nat. Commun.* **8**, 14997 (2017).
24. J. Kim, E. Cha, J. Park, Recent advances in smart contact lenses. *Adv. Mater. Technol.* **5**, 1900728 (2020).
25. J. Kim, J. Kim, M. Ku, E. Cha, S. Ju, W. Y. Park, K. H. Kim, D. W. Kim, P.-O. Berggren, J.-U. Park, Intraocular pressure monitoring following islet transplantation to the anterior chamber of the eye. *Nano Lett.* **20**, 1517–1525 (2020).
26. L. K. Banbury, "Stress biomarkers in the tear film," thesis, Southern Cross University, Lismore, NSW (2009).
27. C. Tlili, N. V. Myung, V. Shetty, A. Mulchandani, Label-free, chemiresistor immunosensor for stress biomarker cortisol in saliva. *Biosens. Bioelectron.* **26**, 4382–4386 (2011).
28. J. Kim, M.-S. Lee, S. Jeon, M. Kim, S. Kim, K. Kim, F. Bien, S. Y. Hong, J.-U. Park, Highly transparent and stretchable field-effect transistor sensors using graphene-nanowire hybrid nanostructures. *Adv. Mater.* **27**, 3292–3297 (2015).
29. M. T. Hwang, M. Heiranian, Y. Kim, S. You, J. Leem, A. Taqieddin, V. Faramarzi, Y. Jing, I. Park, A. M. van der Zande, S. Nam, N. R. Aluru, R. Bashir, Ultrasensitive detection of nucleic acids using deformed graphene channel field effect biosensors. *Nat. Commun.* **11**, 1543 (2020).
30. B. Cai, S. Wang, L. Huang, Y. Ning, Z. Zhang, G.-J. Zhang, Ultrasensitive label-free detection of PNA–DNA hybridization by reduced graphene oxide field-effect transistor biosensor. *ACS Nano* **8**, 2632–2638 (2014).
31. T.-Y. Chen, P. T. K. Loan, C.-L. Hsu, Y.-H. Lee, J. T.-W. Wang, K.-H. Wei, C.-T. Lin, L.-J. Li, Label-free detection of DNA hybridization using transistors based on CVD grown graphene. *Biosens. Bioelectron.* **41**, 103–109 (2013).
32. E. Fernandes, P. D. Cabral, R. Campos, G. Machado Jr., M. F. Cerqueira, C. Sousa, P. P. Freitas, J. Borme, D. Y. Petrovykh, P. Alpuim, Functionalization of single-layer graphene for immunoassays. *Appl. Surf. Sci.* **480**, 709–716 (2019).
33. H. Tao, M. A. Brenckle, M. Yang, J. Zhang, M. Liu, S. M. Siebert, R. D. Averitt, M. S. Mannoor, M. C. McAlpine, J. A. Rogers, D. L. Kaplan, F. G. Omenetto, Silk-based conformal, adhesive, edible food sensors. *Adv. Mater.* **24**, 1067–1072 (2012).
34. J. Kim, A. Banks, Z. Xie, S. Y. Heo, P. Gutruf, J. W. Lee, S. Xu, K.-I. Jang, F. Liu, G. Brown, J. Choi, J. H. Kim, X. Feng, Y. Huang, U. Paik, J. A. Rogers, Miniaturized flexible electronic systems with wireless power and near-field communication capabilities. *Adv. Funct. Mater.* **25**, 4761–4767 (2015).
35. G. E. Dunbar, B. Shen, A. Aref, The Sensimed Triggerfish contact lens sensor: Efficacy, safety, and patient perspectives. *Clin. Ophthalmol.* **11**, 875–882 (2017).
36. S. Cheng, Z. Wu, A microfluidic, reversibly stretchable, large-area wireless strain sensor. *Adv. Funct. Mater.* **21**, 2282–2290 (2011).
37. J. Mujal, E. Ramon, E. Díaz, J. Carrabina, Á. Calleja, R. Martínez, L. Terés, Inkjet printed antennas for NFC systems, in *17th IEEE International Conference on Electronics, Circuits and System* (IEEE, 2010), pp. 1220–1223.
38. J. Jang, B. G. Hyun, S. Ji, E. Cho, B. W. An, W. H. Cheong, J.-U. Park, Rapid production of large-area, transparent and stretchable electrodes using metal nanofibers as wirelessly operated wearable heaters. *NPG Asia Mater.* **9**, e432 (2017).
39. M. H. Tooley, M. H. Tooley, *Electronic Circuits: Fundamentals and Applications* (Elsevier, ed. 3, 2006), pp. 77–78.
40. Y.-G. Park, H. Min, H. Kim, A. Zhexembekova, C. Y. Lee, J.-U. Park, Three-dimensional, high-resolution printing of carbon nanotube/liquid metal composites with mechanical and electrical reinforcement. *Nano Lett.* **19**, 4866–4872 (2019).
41. Y.-G. Park, H. S. An, J.-Y. Kim, J.-U. Park, High-resolution, reconfigurable printing of liquid metals with three-dimensional structures. *Sci. Adv.* **5**, eaaw2844 (2019).
42. J. Park, J. Kim, S.-Y. Kim, W. H. Cheong, J. Jang, Y.-G. Park, K. Na, Y.-T. Kim, J. H. Heo, C. Y. Lee, J. H. Lee, F. Bien, J.-U. Park, Soft, smart contact lenses with integrations of wireless circuits, glucose sensors, and displays. *Sci. Adv.* **4**, eaap9841 (2018).
43. IEEE standard for safety levels with respect to human exposure to radio frequency electromagnetic fields, 3 kHz to 300 GHz, in *IEEE Std C95.1-2005 (Revision of IEEE Std C95.1-1991)* (IEEE, 2006), pp. 1–238.
44. A. Comin, V. Zufferli, T. Peric, F. Canavese, D. Barbetta, A. Prandi, Hair cortisol levels determined at different body sites in the New Zealand White rabbit. *World Rabbit Sci.* **20**, 149–154 (2012).
45. E. J. Holland, M. J. Mannis, W. B. Lee, *Ocular Surface Disease: Cornea, 158 Conjunctiva and Tear Film* (Elsevier/Saunders, London, 2013), 159 pp.
46. American Society for Testing Materials, Standard Guide for Accelerated Aging of 160 Sterile Barrier Systems for Medical Devices. ASTM F1980-07 (2011).

Acknowledgments

Funding: This work was supported by the Ministry of Science and ICT (MSIT) and the Ministry of Trade, Industry and Energy (MOTIE) of Korea through the National Research Foundation (2019R1A2B5B03069358 and 2016R1A5A1009926), the Bio & Medical Technology Development Program (2018M3A9F1021649), the Nano Material Technology Development Program (2015M3A7B4050308 and 2016M3A7B4910635), and the Industrial Technology Innovation Program (10080577). In addition, we thank the Institute for Basic Science (IBS-R026-D1) for financial support and the Research Program (2018-22-0194) funded by Yonsei University. **Author contributions:** M.K. and J.K. wrote the manuscript, performed the experiments, and analyzed the data. W.K. and H.H.L. performed the fabrication of the cortisol antibody and antigen, and J.-E.W., J.-H.L., and J.C. were responsible for the experiments on biocompatibility. Y.-G.P. contributed to the fabrication of the lens devices and FTIR measurement, and J.P. participated in the sensor stability experiments. J.-H.L. and J.C. established the experimental setup and facilities. J.-U.P. oversaw all the research phases. All of the authors discussed and commented on the manuscript. **Competing interests:** The authors declare that they have no competing interests. **Data and materials availability:** All data needed to evaluate the conclusions in the paper are present in the paper and/or the Supplementary Materials. Additional data related to this paper may be requested from the authors.

Submitted 13 February 2020
Accepted 26 May 2020
Published 8 July 2020
10.1126/sciadv.abb2891

Citation: M. Ku, J. Kim, J.-E. Won, W. Kang, Y.-G. Park, J. Park, J.-H. Lee, J. Cheon, H. H. Lee, J.-U. Park, Smart, soft contact lens for wireless immunosensing of cortisol. *Sci. Adv.* **6**, eabb2891 (2020).